A&A 505, 1007–1016 (2009)
DOI: 10.1051/0004-6361/200912015

Astronomy & Astrophysics

Uncovering strong MgII absorbing galaxies

Imaging below the Lyman limit⋆

L. Christensen[1], P. Noterdaeme[2], P. Petitjean[3], C. Ledoux[4], and J. P. U. Fynbo[5]

[1] European Southern Observatory, Karl-Schwarzschild-Strasse 2, 85748 Garching, Germany
e-mail: lichrist@eso.org
[2] Inter-University Centre for Astronomy and Astrophysics, Post Bag 4, Ganeshkhind, 411007 Pune, India
e-mail: pasquiern@iucaa.ernet.in
[3] UPMC Paris 6, Institut d'Astrophysique de Paris, UMR7095 CNRS, 98bis Bd Arago, 75014 Paris, France
e-mail: petitjean@iap.fr
[4] European Southern Observatory, Alonso de Córdova 3107, Casilla 19001, Vitacura, Santiago 19, Chile
e-mail: cledoux@eso.org
[5] Dark Cosmology Centre, Niels Bohr Institute, University of Copenhagen, Juliane Maries Vej 30, 2100 Copenhagen Ø, Denmark
e-mail: jfynbo@astro.ku.dk

Received 9 March 2009 / Accepted 8 August 2009

ABSTRACT

Context. The nature of the galaxies that give rise to absorption lines, such as damped Lyman-α systems (DLAs) or strong Mg II lines, in quasar spectra is difficult to investigate in emission. These galaxies can be very faint and located close to the lines of sight of the much brighter background quasars.
Aims. Taking advantage of the total absorption of the QSO light bluewards of the Lyman limit of two DLAs at $z > 3.4$, we look for the continuum emission from intervening galaxies at $z \approx 2$ that are identified via strong metal absorption lines. The Mg II absorbers have equivalent width large enough to be potential DLA systems.
Methods. Deep images are obtained with the FOcal Reducer and Spectrograph (FORS1) on the Very Large Telescope for the fields towards SDSS J110855+120953 and SDSS J140850+020522. These quasars have Mg II absorption lines at $z = 1.87$ (W_r(Mg II) = 2.46 Å) and $z = 1.98$ (W_r(Mg II) = 1.89 Å), respectively, and each QSO has two intervening higher redshift DLAs at $z > 3$. The U and R bands of FORS1 lie blue and redwards of the Lyman limit of the background DLAs, allowing us to search for emission from the foreground galaxies directly along the lines of sight to the QSOs.
Results. No galaxies are found close to the sight line of the QSO to a point source limit of $U_{AB} \sim 28.0$. In both fields, the closest objects lie at an impact parameter of ∼5″ corresponding to ∼40 kpc in projection at $z = 2$, and have typical colours of star forming galaxies at that redshift. However, the currently available data do not allow us to confirm if the galaxies lie at the same redshifts as the absorption systems. A more extended structure is visible in the SDSS J14085+020522 field at an impact parameter of 0.″8 or 7 kpc. If these objects are at $z \approx 2$ their luminosities are 0.03–0.04 L^* in both fields. The star formation rates estimated from the UV flux are 0.5–0.6 $M_\odot$ yr^{-1}, while the SFRs are half these values if the U band flux is due to Lyα emission alone.
Conclusions. The non-detection of galaxies near to the line of sight is most likely explained by low metallicities and luminosities of the Mg II galaxies. Alternatively, the Mg II clouds are part of extended halos or in outflows from low-metallicity galaxies.

Key words. cosmology: observations – galaxies: high-redshift – quasars: absorption lines – quasars: individual: SDSS J110855.46+120953.3 – quasars: individual: SDSS J140850.91+020522.7

1. Introduction

During the past decade much information has been gathered about the properties of high redshift galaxies from the surveys of Lyman break galaxies (LBGs; Steidel et al. 1995, 2003). Since their detection requires the galaxies to have relatively bright continuum emission, the Lyman break technique preferentially selects massive galaxies (Erb et al. 2006b), and follow up spectroscopy have revealed relatively metal rich galaxies (0.4–0.8 solar in Erb et al. 2006a). Alternatively, the spectra of high redshift quasars can reveal the existence of much fainter and more metal poor galaxies through intervening absorption lines. Strong H I absorption lines with column densities in the damped Lyman-α (DLA) regime ($\log N$(H I) (cm^{-2}) ≥ 20.3) are believed to arise when the sight line toward a QSO intersects a gas rich galaxy (Wolfe et al. 1986, 2005).

Metal absorption lines indicate typical DLA metallicities between one hundredth and one tenth solar (Pettini et al. 1999; Prochaska et al. 2002). The velocity profiles of the lines (Prochaska & Wolfe 1997) can be explained by the complex dynamics of infalling clumps in a merging scenario (Haehnelt et al. 1998; Ledoux et al. 1998; Nagamine et al. 2007). Numerical simulations reproduce reasonably well the kinematics for $z = 3$ DLAs in a hierarchical model (Pontzen et al. 2008), where gas is later distributed in discs at $z = 0$. Comparisons of local H I discs with DLAs at $z > 2$ have indicated that local H I discs have different kinematics than high redshift DLAs (Zwaan et al. 2008), which may indicate that some DLAs could arise in starburst winds or debris from tidal interactions. Winds may not be

⋆ Based on observations collected at the European Southern Observatory, Chile, under programme IDs 380.A-0350 and 080.A-0482.

solely responsible for the large velocities indicated by the absorption lines. Observations have indicated a relation between the velocity width of the metal absorption lines and DLA metallicity (Ledoux et al. 2006), which has been reproduced by numerical simulations (Pontzen et al. 2008). In one DLA towards Q0458-020, the velocity difference between the absorption lines and the Lyα emission line seen in the DLA trough is consistent with a rotating disc (Heinmüller et al. 2006). In most cases, no Lyα emission lines are found in the DLA trough, so whether the star formation activity and supernovae that produce the metals occur in situ (Wolfe et al. 2004) at the time of the spectroscopic observation of the DLA, still has to be verified observationally. High redshift DLA systems might also be affected by galactic winds that remove the neutral gas from the galaxies in competition with accretion from the intergalactic medium (Bond et al. 2001; Prochaska & Wolfe 2009; Tescari et al. 2009). Combining measurements of star formation rates (SFRs) and impact parameters for the galaxies with metallicities and velocities determined from the absorption lines, is needed in order to disentangle these effects.

In contrast to LBGs, the galaxy counterparts of DLAs are selected independently of their luminosities. To date ~1000 DLA systems are known from the SDSS spectra (Prochaska et al. 2005; Noterdaeme et al. 2009). Yet, despite intense observational efforts in the past couple of decades, only four $z > 2$ DLA galaxies have been found in emission (Møller et al. 2002, 2004). The main difficulty is detecting the galaxies against the glare of the bright background QSO, where the continuum emission from the galaxies may be 10 mag fainter than the background source. High resolution images from the HST have revealed faint ($H_{\rm AB} \sim 25$) objects typically 1–2″ in projection from the QSOs studied (Warren et al. 2001), but without redshift information, it is not known whether these are the galaxy counterparts to the DLAs. Other techniques exploit the total absorption of the QSO emission at the wavelength of Lyα in the DLA. If the absorbing galaxies are forming stars, they should be detectable as Lyα emitters and through the UV continuum emission from their young stellar populations. Narrow band images have provided a few detections of Lyα emission (Smith et al. 1989; Wolfe et al. 1992; Møller & Warren 1993) as well as a few upper limits (Grove et al. 2009) close to the sight lines of QSOs. Some candidate Lyα emitters are found at the redshift of the DLAs with integral field spectroscopy (Christensen et al. 2007), while strong limits on the Lyα flux from DLA galaxies have been obtained with Fabry-Perot images (Kulkarni et al. 2006). DLA galaxies are fainter and have smaller SFRs than typical LBGs (Fynbo et al. 1999; Colbert & Malkan 2002; Wolfe & Chen 2006; Fynbo et al. 2008). Very deep spectroscopic observations of Lyα emission from candidate DLA galaxies gives typical SFRs of a few tenths of solar masses per year where the Lyα emission can be extended over a few tens of kpc (Rauch et al. 2008). The DLA galaxies are therefore challenging to detect even with the largest telescopes.

Another method to detect the galaxies in emission takes advantage of sight lines with multiple intervening strong absorbers. If the highest redshift absorber has a hydrogen column density much larger than 10^{17} cm^{-2}, defining a Lyman limit system (LLS), all the flux from the QSO bluewards of the Lyman break ($\lambda = 912(1 + z)$ Å) is absorbed. This idea was originally exploited in the search for high redshift galaxies towards luminous QSOs (Steidel & Hamilton 1992). If the sight line has a lower redshift absorber, the emission from its associated galaxy will be visible even directly in front of the QSO, or at a very small impact parameter. O'Meara et al. (2006) observed strong Mg II absorbers at $z \sim 2$ seen in QSO spectra which had higher redshift LLS, and found two bright L^* galaxies at projected distances of 12–16 kpc to the two QSOs. Several studies have aimed to identify the host galaxies of strong Mg II systems, mostly at lower redshifts $z \lesssim 1$. The presence of galaxies responsible for absorption lines at impact parameters of 20–40 kpc is used to argue for starburst driven winds (Nestor et al. 2007; Bouché et al. 2007), but such winds are not necessary in a model where the extended gaseous halos follow a Holmberg relation (Steidel 1995; Kacprzak et al. 2008; Chen & Tinker 2008).

Gamma-ray burst (GRB) afterglows have recently proven to be of similar use as QSOs for the study of intervening absorption systems. GRBs have the advantage that the afterglows fade away providing a clear line of sight for the absorbing galaxies. In a several cases, galaxies which are possibly responsible for intervening strong Mg II absorption lines have been found within an impact parameter of ~10 kpc from the line of sight to the afterglow (Jakobsson et al. 2004; Chen et al. 2009; Pollack et al. 2009). These intervening galaxies have luminosities in the range 0.1–1 L^*. The discrepancy between the impact parameters and luminosities found for galaxy counterparts of QSO– and GRB Mg II absorbers could suggest that bright background QSOs prevent us from detecting potentially fainter galaxies closer to their lines of sight.

In this paper we exploit the absorption of the UV light of two high redshift QSOs that have multiple intervening absorption systems in their spectra. The observations in the two fields reach an unprecedented depth with a detection limit of 0.03 L^* in the U band. This allows us to put strong constraints on the SFRs directly in the QSO lines of sight. Throughout the paper, we assume a flat cosmology with $\Omega_M = 0.3$, $\Omega_\Lambda = 0.7$ and $H_0 = 72$ km s^{-1} Mpc^{-1}.

2. Observations

2.1. Sample selection

While Lyman limit systems with H I column densities of 10^{17} cm^{-2} are optically thick bluewards of the Lyman limit, some of the background emission is transmitted, and only at higher column densities where the optical depth is sufficient (N(H I)> 10^{19} cm^{-2}) will the blue wavelengths be completely absorbed. A QSO with a DLA system at $z > 3.39$ will have all its emission absorbed in the U band. An intervening galaxy with a redshift in the range $1.7 < z < 2.3$ will have a Lyα emission line in the U band provided it is forming stars. Meanwhile, the faint emission will be observable from the ground and its emission properties will be completely unaffected by the bright background QSO. This effective approach to locate the galaxies responsible for intervening strong absorption lines (including DLAs), near bright QSOs is demonstrated in O'Meara et al. (2006).

To find such configurations, we systematically searched the Sloan Digital Sky Survey spectra of about 2000 QSOs for $z > 3.5$ DLAs in the data release 5 (Schneider et al. 2007). To ensure that no flux was present from the QSO and that the Lyα emission line was well within the transmission function of the U band, the redshift criteria were chosen to be conservative. Because the QSO emission around the Lyα line of lower redshift galaxies is completely absorbed it is not possible to determine the hydrogen column density. Instead we used the strong Mg II $\lambda\lambda$2796, 2803 doublet as a proxy for selecting DLAs. These strong lines are easy to identify in QSO spectra, and can be used to identify low redshift DLAs where only few have measured hydrogen

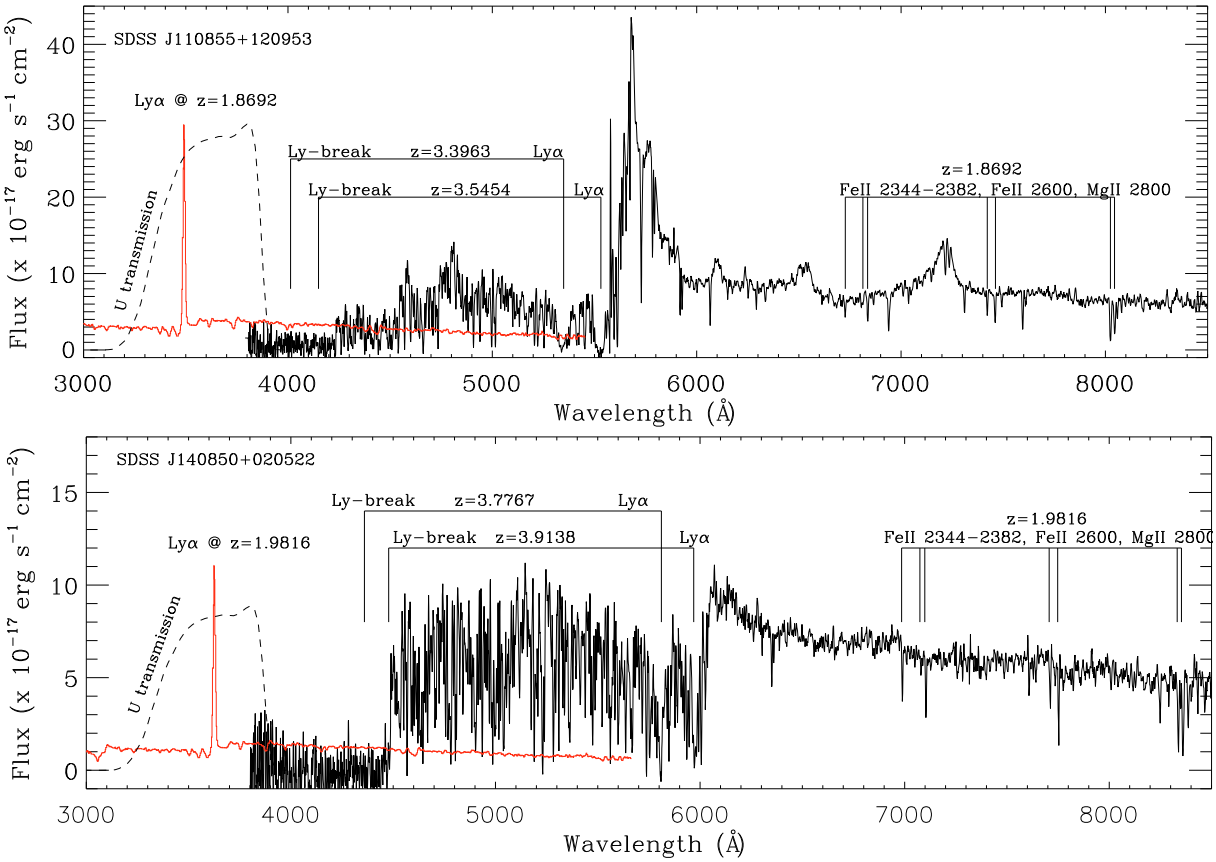

Fig. 1. Sloan spectra of the two quasars. In each quasar spectrum, two DLAs (at $z_{\rm DLA}$ = 3.5454 and 3.3963 for SDSS J110855.46+120953.3, *upper panel*, and $z_{\rm DLA}$ = 3.9138 and 3.7767 for SDSS J140850.91+020522.7, *lower panel*) completely absorb the QSO emission bluewards of 4200 Å. Two lower redshift systems are identified through their strong metal absorption lines. Both panels indicate the transmission curve of the *U* band, which lies bluewards of the absorption cutoffs. Spectra of Lyman break galaxies with Lyα in emission (Shapley et al. 2003) at the redshifts of the Mg II absorption systems are indicated in the two plots. Their Lyα emission lines fall within the *U* band in both cases.

column densities (Rao & Turnshek 2000; Rao et al. 2006). It is not known if strong Mg II absorbers are identical to DLAs; absorbers with Mg II equivalent widths larger than 0.6 Å and lines spread over more than 300 km s^{-1} only have a probability of ∼50% of being DLAs (Ellison et al. 2009). SDSS Spectra with at least one high redshift DLA system were investigated further to find Mg II $\lambda\lambda$2796,2803 absorption lines with a rest frame equivalent width ($W_{\rm r}$) larger than 0.6 Å at $1.75 < z < 2.2$, where the redshift limits ensure that the associated Lyα emission line fall within the FORS *U* band. These criteria were met by two equatorial QSOs (SDSS J110855+120953 at z = 3.671 and SDSS J140850+020522 at z = 4.008) which could be observed by the VLT. Hereafter, we shall refer to these two QSOs as Q1108, and Q1408. The SDSS spectra of the two QSOs are shown in Fig. 1. By coincidence both targets had two intervening DLAs in addition to the strong Mg II system, which effectively absorb all of the QSO emission immediately bluewards of the redshifted Lyman limit break.

In each spectrum, the lower redshift absorption system is detected by several metal absorption lines in addition to the Mg II $\lambda\lambda$2796,2803 doublet. Table 1 lists the properties of the absorption systems. The high $W_{\rm r}$ measured for the metal lines suggest that the strong metal absorption systems are possibly DLAs. At $W_{\rm r}^{\rm Mg\,II\lambda2852} > 0.6$ Å, combined with a criterion for the fraction $W_{\rm r}^{\rm Mg\,II\lambda2796}/W_{\rm r}^{\rm Fe\,II\lambda2600} < 2$, more than 50% of the systems are DLAs (Rao et al. 2006). This is consistent with the analysis of the Mg II absorption line velocity spread discussed in Sect. 5.1.

Table 1. Absorption line systems in the two QSO spectra.

	$z_{\rm QSO}$	$z_{\rm DLA,1}$	$z_{\rm DLA,2}$	$z_{\rm Mg\,II}$	$W_{\rm r}^{\rm Fe\,II\lambda2600}$ (Å)	$W_{\rm r}^{\rm Mg\,II\lambda2796}$ (Å)	$W_{\rm r}^{\rm Mg\,I\lambda2852}$ (Å)
Q1108	3.671	3.5454	3.3963	1.8692	1.23	2.46	0.61
Q1408	4.008	3.9138	3.7767	1.9816	0.97	1.89	

The metal line rest frame $W_{\rm r}$ are measured for the lowest redshift systems in the SDSS spectrum for Q1408, and the UVES data for Q1108. The SDSS spectra give values consistent within the uncertainties with the UVES data. The SDSS spectrum of Q1408 is too noisy to identify the Mg I line.

2.2. Photometry

The two fields were observed with the blue sensitive CCD on VLT/FORS1 taking advantage of the high transmission of a new *U* filter (*U*-high), which transmits almost 90% at its peak sensitivity around 3800 Å. We obtained very deep observations in the *U* band (4.6 and 5.4 h on target, respectively, divided into jittered exposures of 980 s), with shorter (450 s) *R* band observations for both fields. The *R* band images helped to pinpoint the exact location of the QSO with respect to the nearby galaxies. The

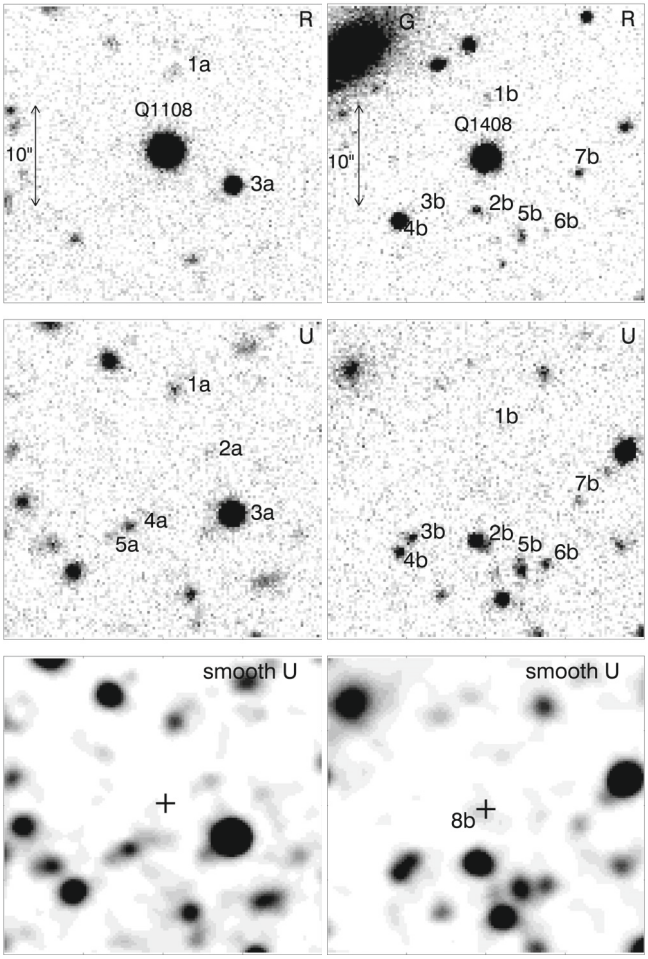

Fig. 2. *R* and *U* band images of Q1108 shown the *left column*, and for Q1408 in the *right*. In the *U* bands the emission from the QSOs have been completely absorbed. The images are 30″ on a side with the orientation north up and east left. Objects within 10″ from the QSOs lines of sight are labeled with numbers and the photometry of these is listed in Table 2. The bottom row shows smoothed version of the *U* band images, with a "+" sign indicating the location of the QSO. Only in the case of Q1408 do we detect an extended object close to the line of sight of the QSO, which is otherwise not detectable in the unsmoothed *U* band.

observations were done in service mode between March 6 and 9, 2008 under photometric conditions and with seeing conditions between 0.″6 and 1″.

The data were reduced with standard procedures, subtracting an average bias frame, and flat fielding using twilight sky frames. The images were registered and combined to reject bad pixels and cosmic ray hits. To optimise the depth of the images in the *U* band, two of the 16 frames of Q1408 were rejected due to poor seeing. The *FWHM* measured from stars in the fields is 0.″8 and 0.″9 in the *R* and *U* band, respectively. Both *U* band images do not show any residual emission from the QSOs. The full field of view of FORS1 is 6.′8×6.′8, but here we focus on the immediate regions around the QSOs, as shown in Fig. 2. The images are 30″ on a side with orientation north up and east left.

Instrumental zero points were estimated from observations of standard stars in the field Rubin 149 obtained on the same nights as the science observations. Transformations from instrumental magnitudes to Vega magnitudes were calculated using `IRAF-PHOTCAL`. The transformation equations from the instrumental to Vega magnitudes included an extinction coefficient appropriate for Paranal (Patat 2003). A potential inclusion of a colour term was consistent with zero to within the uncertainties, so this term was neglected. Magnitude uncertainties were propagated through the equations. Aperture photometry showed that within a 1″ radial aperture, the 3σ significance detection limit was $U_{\rm Vega} = 27.3$ mag for a point source in both fields, while the 3σ significance limit in the *R* band was shallower: 26.4 mag and 26.5 mag (Vega) for Q1108, and Q1408, respectively. The magnitudes were corrected for Galactic extinction (Schlegel et al. 1998). Transformations from the Vega to AB magnitudes were calculated from the filter transmission curve and the spectrum of Vega (Fukugita et al. 1995). For the FORS1 filters we calculated $U_{\rm AB} = U_{\rm Vega} + 0.66$ and $R_{\rm AB} = R_{\rm Vega} + 0.18$ mag. We use the AB magnitudes unless otherwise stated.

Since the *U* band images were the deepest they were used primarily to detect objects. The locations were cross checked with object detection in the *R* band to avoid missing any *U* band dropout.

2.3. High resolution spectra

In addition to the imaging data we took advantage of one 4200 s integration of Q1108 with VLT+UVES obtained as a part of another observing programme (ID 080.A-0482, PI: Sebastian Lopez). The data were used to study the velocity widths of the strong Mg II absorption lines as described in Sect. 5.1.

Both the blue and red UVES spectrograph arms were used simultaneously with standard dichroic settings, with central wavelength of 437 and 860 nm. The resulting wavelength coverage is 305 to 1042 nm with gaps at 575–583 nm and 852–866 nm. The CCD pixels were binned by a factor of 2 × 2 and the slit width adjusted to 1″. This yielded a resolving power of 48 000 under the seeing conditions of 1″.

The data were reduced using the ESO pipeline system, which allowed for an accurate extraction of the object spectrum, while subtracting the sky spectrum and removing cosmic ray hits and CCD defects at the same time. Wavelengths were finally shifted to the vacuum-heliocentric rest frame. The signal-to-noise ratio in the reduced spectrum was measured to be 15–20 per pixel.

3. Observational results

3.1. Nearby galaxies and colours

The goal of this study is to detect objects located directly along the QSO line of sight. In both fields the closest objects lie at a separation of ∼5″ from the QSO. If either of these galaxies are responsible for the strong absorption line system seen in the QSO spectra, the projected separation is ∼40 kpc at the redshift of the absorbers. No other nearby objects are found at the 3σ significance level (corresponding to 0.03 L^*). At $z = 2$ a luminous L^* galaxy has an absolute magnitude of $U^*_{\rm AB} = -21.9$ mag (Gabasch et al. 2004), and an observed magnitude of $U_{\rm AB} = 24.0$ mag in the adopted cosmology. The numbered objects in Fig. 2 mark all galaxies that are located within 10″ of the QSO; most of these objects are fainter than $U = 24$ mag. The photometry of these galaxies is listed in Table 2.

We investigate whether the colours are similar to other galaxies detected in galaxy surveys. For comparison we use photometry of galaxies from the GOODS-MUSIC catalog (Grazian et al. 2006) where multiband photometry allows an accurate determination of the photometric redshift. To estimate the $R_{\rm AB}$ magnitude of the GOODS galaxies, we linearly interpolate the flux between the measured *F*606*W* and *F*775*W* bands to calculate the

Table 2. Vega magnitudes of objects identified within ∼10″ from the QSO lines of sight, with the observed offsets in RA and Dec (in arcsec), and projected impact parameter (in arcsec).

Object no.	Offset (″)		b (″)	U (mag)	R (mag)	L_U/L_U^* at $z = 2$
Q1108						
1a	0.7 E	8.4 N	8.4	25.83 ± 0.10	25.41 ± 0.18	0.10
2a	4.1 W	2.4 N	4.7	27.06 ± 0.28	>26.4	0.03
3a	6.4 W	3.4 S	7.2	22.66 ± 0.01	22.23 ± 0.02	1.87
4a	3.4 E	4.8 S	5.8	25.88 ± 0.11	>26.4	0.10
5a	5.3 E	5.2 S	7.4	26.75 ± 0.28	>26.4	0.03
Q1408						
1b	0.0 E	6.4 N	6.4	>27.3	25.82 ± 0.25	<0.03
2b	1.0 W	5.4 S	5.5	24.64 ± 0.04	24.81 ± 0.10	0.31
3b	6.9 E	5.0 S	8.5	25.75 ± 0.09	25.64 ± 0.20	0.11
4b	8.2 E	6.4 S	10.4	25.55 ± 0.07	22.25 ± 0.02	0.13
5b	3.3 W	8.2 S	8.9	25.53 ± 0.08	24.79 ± 0.10	0.13
6b	5.6 W	7.7 S	9.5	26.03 ± 0.12	26.41 ± 0.40	0.08
7b	8.8 W	1.7 S	8.9	26.73 ± 0.21	24.88 ± 0.10	0.04
8b	0.7 E	0.3 S	0.8	26.92 ± 0.10	–	0.04

Objects near Q1108 are in the upper 5 rows, and near Q1408 in the bottom 8 rows. The magnitudes are corrected for Galactic extinction. The last column gives the luminosity fraction relative to a U^* galaxy at $z = 2$, which has an apparent magnitude $U_A = 24$. The uncertainties are 0.01 for this fraction.

flux at 6440 Å. We are mainly interested in the observed colours of galaxies around $z = 2$, where the HST bands correspond to restframes 2000 and 2580 Å, respectively. Between wavelengths 1500–2800 Å galaxy spectra are mostly flat when measured in frequency units, f_ν (Kennicutt 1998), so a simple interpolation to calculate the R band magnitude is well justified. The transmission curves for the VIMOS U band used in the GOODS-MUSIC catalog is different from the FORS1 high transmission U filter. We calculate a transformation between the two systems: $U_{\rm FORS1} = U_{\rm VIMOS} + 0.04$ mag.

A colour-magnitude diagram of ∼1000 galaxies with photometric redshifts between 1.8 and 2.3 is shown as a grey scale image in Fig. 3. Galaxies detected in the two QSO fields with a signal-to-noise ratio >3 are shown as small symbols, and the objects detected within 10″ are shown as larger symbols with error bars. Due to our shallower R band observations relative to the GOODS observations, objects in the lower right hand corner are undetected in our observations. The colours of the GOODS galaxies span a narrower range than for the galaxies in the two QSO fields, where there is an excess of galaxies with colours around $U - R > 1.5$. If no photometric redshift selection is made for the GOODS galaxies, a wider range of colours are found, and the two colour distributions are consistent.

The typical colour of an irregular galaxy, calculated from template spectra (Kinney et al. 1996), and redshifted to $z = 2$ is shown as a diamond, where its U band magnitude correspond to an L^* galaxy. By creating artificial spectra of metal poor, young galaxies (Bruzual & Charlot 2003) with an additional intrinsic extinction of $A_V = 0.5$ mag, we estimate the colour and magnitude change. We also calculate the colour and magnitude change if the galaxies have strong Lyα emission with a rest frame equivalent width of 100 Å. The arrows in Fig. 3 show the respective changes which are minor. More evolved galaxies have redder colours ($U - R > 3$) independently of the metallicity and the initial mass function of the galaxy templates. This implies that the entire range of colours in Fig. 3 can be obtained for high redshift galaxies. Specifically, the red colour of object no. 4b in the Q1408 field is consistent with an evolved galaxy at $z \approx 2$ with an age greater than 700 Myr for the dominant population of stars. In the Q1408 field there are several red galaxies present at impact parameters larger than 10″ from the QSO line of sight. In the upper right hand panel of Fig. 2, the R band image of Q1408, a large and bright galaxy is partly visible (marked "G") in the image. This galaxy has the morphology and colours of a low redshift elliptical, and there are several fainter galaxies with the same colours around it. It is likely that object no. 4b is part of a lower redshift group environment.

Although there are no clear correlations between the $U - R$ colour and redshift, objects with $U - R < 0.5$ are more likely to lie at $z > 0.9$. 52% of the GOODS galaxies fulfill these criteria, while only 20% of galaxies at $z < 0.9$ have such blue colours. However, the single $U - R$ colour is insufficient to make an exact redshift estimate, and not good at all to select objects at $z \sim 2$. Additional observations in the V band would be useful to apply the BM/BX colour criterion to select galaxies with $1.4 < z < 2$ (Adelberger et al. 2004).

Objects no. 2b, 3b and 6b in the Q1408 field and no. 4a in the Q1108 field have the bluest colours. Given their non-detection in the R band, several of the objects could potentially be located at higher redshifts with very blue colours.

3.2. Extended objects

To check for the presence of extended low surface brightness objects closer to the lines of sight of the QSOs, the U band images are convolved with Gaussian point spread functions with a $FWHM$ of 1.″5 and 2″, respectively. While the 3σ detection limit is $U_{\rm AB} = 28.0$ for a point source, the smoothed images have a deeper 3σ detection limit of $U_{\rm AB} = 28.5$ within a 1.″5 radial aperture for the two fields. No objects are detected close to the line of sight of the QSO in the field of Q1108. Objects 4a and 5a in the Q1108 field have a separation of 2″, and appear merged into one elongated object in the smoothed image. Furthermore there is an extension of emission to the west of object no. 4a which is not directly visible in the original image. This extension reaches a minimum impact parameter of 3.″8 directly south of the QSO with a size of 1.″5×3″ and has a magnitude of $U_{\rm AB} = 27.4 \pm 0.1$. If the object is at $z \approx 2$, the projected distance is 31 kpc.

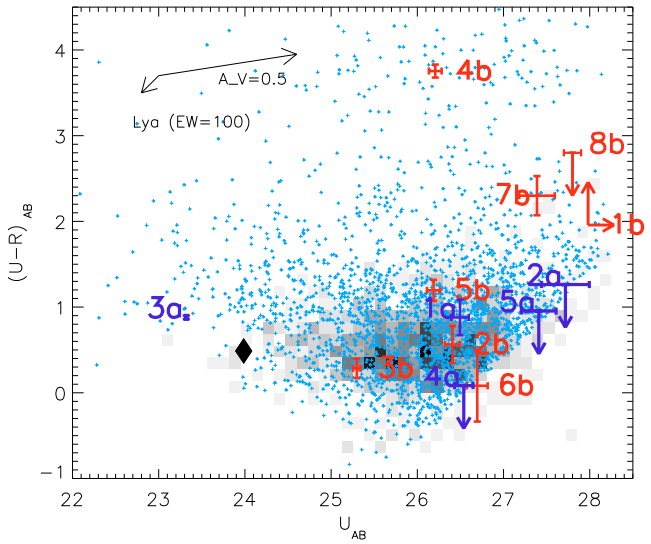

Fig. 3. Colour-magnitude diagram of the objects in the two fields (small plus signs). The grey scale image shows the distribution of ∼1000 galaxies with photometric redshifts $1.8 < z_{\rm phot} < 2.3$ from the GOODS-MUSIC survey. The large crosses with error bars mark the galaxies near to the QSO lines of sight and the numbers refer to those in Table 2 (red symbols for Q1408, and purple for Q1108). The large black diamond symbol shows the colour of an L^* starburst galaxy at $z = 2$. *See the online edition of the journal for a colour version of this figure.*

In the Q1408 field, a faint object ($U_{\rm AB} \sim 27.6 \pm 0.1$ mag within a radial aperture of 1.″5) is detected at an offset of 0.″8 to the south-east of the QSO as displayed in Fig. 2, and labeled as object no. 8b. At $z = 2$ the projected distance is 7 kpc. The object appears elongated with a size of about 2.″5 × 2″ in the frame with a Gaussian convolution width of 1.″5. To estimate whether a faint object is present also in the R band, the QSO is subtracted using the brighter field stars as PSF reference. No additional point sources were visible after the subtraction. To estimate the detection limit of a resolved object against the glare of the brighter QSO, we add artificial objects nearby the bright QSO, and then subtract the PSF to recover the artificial object. These experiments show that we can recover an object with a $FWHM$ of 1.″5 and $R = 25$ mag at a distance of 0.″8 by PSF subtraction. This places a rough upper limit on the colour: $U - R < 2.8$ for the object no. 8b.

3.3. High redshift DLA host galaxies?

In the previous sections we investigated whether some of the spatially nearby galaxies are the hosts of the $z = 2$ Mg II absorption systems, but a related question is whether some of the galaxies could be the hosts of the $z > 3$ DLA systems.

For both fields, the two high redshift DLAs absorb all emission immediately bluewards of the Lyman break. This suggests that the objects detected in the U band images are not likely to be the host galaxies of the $z > 3$ DLA systems because no UV emission bluewards of the Lyman limit break should be able to escape the cloud, at least along the QSOs line of sight. Only object no. 1b in Q1408 is detected in the R band but not in the U band, and this could potentially be the host of one of the DLAs. However, the impact parameter is quite large (44 kpc at $z \approx 3.8$) compared to a typical value of ∼10 kpc found for the few confirmed DLA galaxies at $z > 2$ (Møller et al. 2002; Weatherley et al. 2005). Numerical models also predict small impact parameters of the order or less than 10 kpc for DLA systems (Nagamine et al. 2007; Pontzen et al. 2008). However, little is currently known about the extension and morphology of gaseous disks around high redshift galaxies from observations.

Even though no UV photons bluewards of the Lyman limit can escape the DLA clouds along the line-of-sight, they can escape along other directions with a smaller optical depth. In such a special gas geometry, the emission from the DLA host galaxies can be detected in both the U and the R bands. If the escape fraction of the galaxies is substantial, the Lyman continuum emission could be still observed, and in the images the galaxy would be visible at some distance from the QSO lines of sight. Assuming an escape fraction $f_{1500}/f_{900} = 2.9$–4.5 as observed for two Lyman break galaxies (Shapley et al. 2006), we can calculate the rest frame flux ratio which corresponds to a colour $(U - R)_{\rm AB} \sim 2.2$. Objects no. 4b and 7b in the Q1408 field have colours consistent with being at a redshift of $z > 3$, but the colours are also consistent with lower redshift evolved galaxies. With $R = 22.25$ mag for object no. 4b, it would have a luminosity of $7L^*$ if it were at $z = 3.8$ relative to an $R^* = -23.0$ galaxy (Gabasch et al. 2006) while 7b would have a luminosity of $0.7\,L^*$. Considering that such bright objects are rare, it is more likely that object no. 4b has a lower redshift, and possibly is a member of a group as discussed above. In addition, object no. 7b would have an impact parameter of 65 kpc at $z = 3.8$. Since the objects are faint for follow up spectroscopy, near-IR images of the field can be used instead to investigate the spectral energy distribution and to determine the photometric redshift. Before such observations are made we cannot claim the detection of the hosts of the DLAs.

4. SFR limits

4.1. SFRs from the UV continuum

The limiting magnitude of $U_{\rm AB} = 28.0$ corresponds to a SFR of 0.6 $M_\odot$ yr^{-1} for a galaxy at $z = 2$. At the redshift of the Mg II absorbers, the U band measures the emission at 1200–1400 Å in the rest frame of the absorbers. To estimate the SFR in the UV region, we extrapolate calibrations from other studies.

The conventional conversion from a UV flux to the SFR (Kennicutt 1998) is valid from 1500–2800 Å, where spectra of star forming galaxies are flat. Bluewards of 1500 Å the flux decreases, so we analyse template spectra to estimate the SFR given the U band flux. We use the template spectra from Bruzual & Charlot (2003) of instantaneous star burst populations with ages <100 Myr and a Salpeter initial mass function. Galaxy template spectra are created with the observed U band magnitude at the redshift of the absorber. The template flux bluewards of 1215 Å is reduced to reflect that 15% of the flux is absorbed in the Lyα forest at $z = 2$ (Dall'Aglio et al. 2009). No Lyα emission is present in the template spectrum. From this template the flux at the rest frame 1500–2800 Å is used to calculate the SFR using the standard conversion (Kennicutt 1998), which has an intrinsic scatter of ∼30%.

The SFR conversion depends also on the age and metallicity of the template for which we have to select appropriate values. Since strong Mg II absorbers have about 50% chance of being DLAs (Rao et al. 2006; Ellison et al. 2009), we use typical low metallicities measured for the DLA population (Wolfe et al. 2005). Models of chemical evolutions of the DLAs at high redshifts show that they are typically a few 100 Myr old (Dessauges-Zavadsky et al. 2004). A notable exception is the

Table 3. Conversion factor A for Eq. (1) calculated for different galaxy template ages and metallicities relative to the solar value, $Z_\odot = 0.02$.

Age	0.02 $Z_\odot$	0.2 $Z_\odot$	0.4 $Z_\odot$	1 $Z_\odot$
10 Myr	1.1	1.3	1.4	1.5
50 Myr	1.7	1.9	2.3	2.9
100 Myr	2.3	2.9	3.7	5.5
200 Myr	3.5	5.1	7.3	14.9

DLA towards Q B2230+02, which has a relatively high metallicity and an age of 3 Gyr (Dessauges-Zavadsky et al. 2007). The conversion from luminosity to SFR is given by

$$\mathrm{SFR}\ (M_\odot\ \mathrm{yr}^{-1}) = A \times 10^{-28} L_\nu \left(\mathrm{erg\ s^{-1}\ Hz^{-1}}\right), \quad (1)$$

where L_ν is the luminosity measured around 1200 Å in the rest frame of the galaxy. For a 100 Myr, 0.2 solar metallicity template, we calculate $A = 2.9$ in Eq. (1). Since the factor A depends on the metallicities and ages of the galaxies, we derive the conversion factor for the SFR using a series of templates of varying ages and metallicities (see Table 3) corresponding to the available template metallicities in Bruzual & Charlot (2003).

If the Lyα emission line is very strong we over estimate the SFR with this procedure, since a pure Lyα line indicates a smaller SFR as described in Sect. 4.2. Hence the SFRs that we give are considered to be conservative.

It is possible that the galaxies responsible for the strong absorption systems are extended low surface brightness objects. We compute the apparent magnitude and UV flux for an object detected at the 3σ significance level as a function of radius. To calculate the limiting magnitude for a signal-to-noise ratio of $S/N = 3$ we use $\mathrm{m_{lim}} = zp - 2.5\log(\mathrm{S/N}\sqrt{n_{\mathrm{pix}}}\sigma/t)$, where zp is the FORS zero point measured in magnitudes, $n_{\mathrm{pix}} = \pi(r/0.25)^2$ is the number of pixels within an aperture radius r (in arcsec), and 0.25 is the plate scale of the CCD ($''$/pixel). σ is the standard deviation of the pixel values measured in the reduced CCD frame, and t is the integration time measured in seconds. Given these values, a point source has with a $FWHM = 1''$ has a radial $n_{\mathrm{pix}} = 2$, which at $z = 2$ corresponds to ~4 kpc in the adopted cosmology. The limiting flux increases with increasing aperture, so for more extended galaxies the SFR limit is less strong.

With the observations, we can place a strong constraint on the SFR for an object located directly in the lines of sight of the QSOs. Figure 4 shows the limiting SFR for the lines of sight to the two QSOs as a function of the radial aperture. At large apertures of $3''$, the SFR limit is within 2 $M_\odot$ yr^{-1} including uncertainties. Compared to typical LBGs which have an average SFR measured from the unobscured UV emission of 8 $M_\odot$ yr^{-1} (Erb et al. 2006a), our observations probe high redshift galaxies which are significantly fainter. Similarly, extended continuum emission from DLA galaxies is not detected in the Hubble ultra-deep field (Wolfe & Chen 2006), possibly due to a smaller star formation efficiency in DLAs relative to LBGs.

Wolfe et al. (2004, 2008) estimate the SFR surface density of DLA galaxies to lie in the range 10^{-2}–10^{-3} $M_\odot$ yr^{-1} kpc^{-2} depending on the state of the neutral gas. These values are represented by the dotted lines in Fig. 4. If the absorbing galaxies we are looking for in emission are similar to the DLA absorption systems investigated by Wolfe et al. (2004) we should be able to detect them if the star formation extends uniformly over the galaxy discs. Only the weakest star-forming DLA galaxies would remain undetected. The non detections indicate that galaxies with extended star formation, specifically at the high rate of 10^{-2} $M_\odot$ yr^{-1} kpc^{-2}, are unlikely to be present in the two QSO lines of sight. Alternatively, a high SFR density in a small dwarf galaxy system with a radius $\lesssim$4 kpc has a SFR below the detection limit.

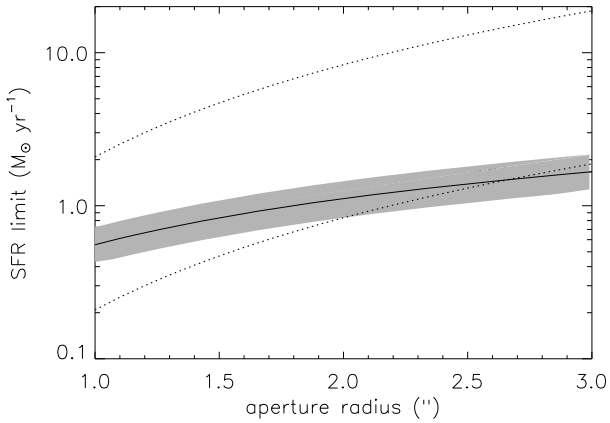

Fig. 4. The limiting SFRs in the two QSO lines of sight (solid line with the uncertainty represented as the shaded area) converted from the limiting magnitude calculated as a function of radial apertures. The limits have been calculated from the original unsmoothed U band images. At $z = 2$ one arcsec corresponds to 8.1 kpc in projection. The upper dotted line shows the average SFR per unit area in DLA galaxies of 10^{-2} $M_\odot$ yr^{-1} kpc^{-2} while the lower dotted line represents a value of 10^{-3} $M_\odot$ yr^{-1} kpc^{-2} corresponding to the lower limit in Wolfe et al. (2004).

The most nearby point source objects (no. 2a,2b in the two fields) have SFR = 0.5 $M_\odot$ yr^{-1} for Q1108 and 4.9 $M_\odot$ yr^{-1} for Q1408, respectively, if they are the absorbing galaxies. The extended object no. 8b near Q1408 has SFR = 0.6 $M_\odot$ yr^{-1}.

4.2. SFRs from Lyα emission

In the hypothetical case that the U band flux comes entirely from a Lyα emission line from the galaxies at $z = 2$, the line flux for the object no. 2a in Q1108 is 2.5×10^{-17} erg cm^{-2} s^{-1}. For Q1408 the line flux is 10.0×10^{-17} erg cm^{-2} s^{-1} and 1.3×10^{-17} erg cm^{-2} s^{-1} for objects no. 2b and 8b, respectively. This in turns corresponds to a SFR of 0.5 $M_\odot$ yr^{-1} for object no. 2a in the Q1108 field and 2.3 $M_\odot$ yr^{-1} and 0.3 $M_\odot$ yr^{-1} for objects no. 2b and 8b near Q1408. To calculate these flux densities, we use the case B recombination scenario (Osterbrock 1989), a flux ratio of Lyα/Hα = 10, and the conversion between Hα luminosity and SFR from Kennicutt (1998). This last assumption of a pure Lyα emission line object is not justified in the case of Q1408, because the continuum emission is detected in the R band, but it serves the purpose of calculating the SFR for comparison to that estimated from the UV continuum.

The Lyα photons are effectively quenched in the presence of dust, so the above SFR are strict lower limits. Since the SFR estimated from the UV is higher than estimated from the Lyα flux by a factor of 3, the unobscured SFR may be somewhere between these values.

We note that the estimated Lyα flux densities and luminosities are in the same range as those measured for the few detections of Lyα emission from DLA galaxies (Møller et al. 2004; Weatherley et al. 2005, and references therein). This is probably not a coincidence, but likely reflects that the searches for emission from DLA galaxies are carried out to the detection limit of currently available instruments.

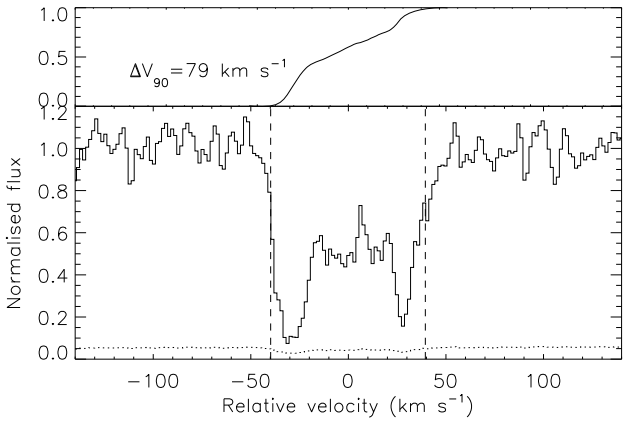

Fig. 5. The *bottom panel* shows the velocity profile of Fe II λ2374 from the UVES data, and the dotted line shows the error spectrum. The *upper panel* demonstrates the integrated, normalised, apparent optical depth, and the vertical dashed lines in the spectrum indicate the wavelengths within which 90% of the absorption is seen.

5. Strong Mg II systems

5.1. Velocity spreads

The UVES data of Q1108 shows a wealth of absorption lines and a detailed analysis will be presented elsewhere. The systemic redshift is found to be $z = 1.8692$ from narrow metal absorption lines of Mg I λ2852 and the Fe II lines. The Mg II $\lambda\lambda$2796,2803 line profiles are complex with several components spread over a velocity of $\Delta v = 308$ km s^{-1}, as typically seen for strong Mg II absorbers (Nestor et al. 2007). The same spread is seen in the C IV λ1549 doublet. The bulk of the Mg II absorption is spread over a smaller velocity range of $\approx$150 km s^{-1} surrounded by weaker satellites at larger velocities. This places the absorber among the strong, but not extremely strong Mg II absorbers. A smaller velocity spread of the dominant absorption components is seen from other non saturated lines such as the Fe II λ2374 line, as demonstrated in Fig. 5. The velocity spread of the Mg II line is twice that suggested by the correlation with the equivalent width Δv (km s^{-1}) ≈ 70 (km s^{-1} Å^{-1})$\times W_r^{\lambda 2796}$ (Å) (Murphy et al. 2007). Using the Mg II absorption line velocity spread to calculate the D-index (Ellison 2006) gives $D = W_r/\Delta v \times 1000 = 8.0$. For values of $D > 7$ the probability that the absorber is a DLA is 50–55% (Ellison et al. 2009).

To compare with previous studies (Ledoux et al. 2006), we measure the velocity spread of the Fe II λ2374 line which satisfies the criterion that the maximum residual emission lies between 0.1 and 0.6 times the continuum level. From the central wavelength defined by the redshift of the system, we measure the velocity range over which 90% of the apparent optical depth (Savage & Sembach 1991) is seen. We find $\Delta V_{90} = 79$ km s^{-1} as demonstrated in Fig. 5. Unsaturated lines typically have smaller velocity spreads relative to the Mg II lines, which may be composed of more components that contribute to the total line width due to their stronger transition.

5.2. Metallicities

Since the Lyα absorption lines corresponding to the Mg II systems lie in the absorbed parts of the QSO spectra, we cannot determine the metallicities as usually done for strong absorption systems. In the absence of an exact metallicity measurement for the Mg II absorbers, we assume that the absorbing clouds are actually DLAs. Consequently, some derivations in this section are only valid if the objects are DLAs, for which the probability is 50%. In case the Mg II absorbers are sub-DLAs we point out the conclusions for this category. We use calibrations and scaling relations found for DLAs and sub-DLAs in the literature to derive the metallicities, and use the conventional notation of the metallicity [M/H] $\equiv \log[N(\mathrm{M})/N(\mathrm{H})] - \log[N(\mathrm{M})/N(\mathrm{H})]_\odot$.

A relation between the metallicity and velocity spread as measured by the ΔV_{90} parameter has been found for DLAs around $z = 2$ (Ledoux et al. 2006). Using this relation and the spread measured from the UVES data of Q1108, the metallicity of the galaxy is expected to be [M/H] = –1.4 ± 0.4. A similar correlation exists for sub-DLAs, for which Dessauges-Zavadsky et al. (2009) suggest a [Fe/H] metallicity which is larger by 0.4–0.6 dex for a given velocity spread. Using [Zn/H] as a tracer of the sub-DLA metallicities, Meiring et al. (2009) find no correlation with velocity, but find systematically larger values for sub-DLAs relative to DLAs.

Another calibration uses the measured values of $W_r^{\mathrm{Si\,II}\lambda 1526}$ which correlates with the metallicity in high redshift DLAs (Prochaska et al. 2008). To use this relation for the Mg II absorber towards Q1108 we need $W_r^{\mathrm{Si\,II}\lambda 1526}$, but that line is strongly contaminated by other absorption lines in the Lyα forest of the QSO. Instead we use the observed relation which suggests that the widths of the lines roughly scale inversely with their wavelengths: $W_r^{\mathrm{Mg\,II}\lambda 2796}/W_r^{\mathrm{Si\,II}\lambda 1526} = 3$ (Prochaska et al. 2008). These relations suggest a metallicity [M/H] = –1.0 ± 0.1 for the Mg II absorber in agreement with the previous metallicity estimate.

These low metallicities are typical for high redshift DLAs (Pettini et al. 1994; Prochaska et al. 2003). Observations have indicated that sub-DLAs have higher metallicities on the average (Péroux et al. 2003; Péroux et al. 2008; Meiring et al. 2009), while an investigation of the redshift dependence demonstrated that this is only true at lower redshifts ($z < 1.7$) (Dessauges-Zavadsky et al. 2009).

5.3. Expected galaxy magnitudes

We can estimate the magnitude for low metallicity galaxies if a luminosity metallicity relation exists for DLA galaxies (Ledoux et al. 2006), again assuming that the clouds are DLAs. A DLA galaxy with 10% solar metallicity is expected to be faint: $R \sim 26.1$ mag or 0.06 L^* at $z = 2$ according to the metallicity–luminosity relation in Ledoux et al. (2006). Such a relation is valid provided the absorption lines velocity spread is used as a proxy for the dark matter halo circular velocity, and there is a direct relation between the halo mass and a galaxy luminosity (Haehnelt et al. 2000). In the case of a lower metallicity ([M/H] = −1.8) the galaxy would be even fainter: $R \sim 30$ mag. Extrapolating this relation to derive magnitudes for sub-DLAs with metallicities as large as [M/H] = −0.4 gives $R = 23.1$. As described in Sect. 3.1, the U–R colour of galaxies at $z = 2$ depends on the age of the most recent dominant starburst, but generally blue colours are expected for young galaxies. Thus, the expected magnitude is $U \sim 26.6$ in the 10% solar metallicity case. Our survey is deeper than this limit, so we would be able to detect the continuum emission from the Mg II galaxies. The non detection of emission within 2″ of line of sight is consistent with the very low metallicity case. If the cloud is a sub-DLA instead, a brighter host galaxy is possible, but since no bright galaxies are found close to the QSO lines of sight, it would have to have a large impact parameter.

Using instead the observed luminosity-metallicity relation either at low (Tremonti et al. 2004) or at higher redshift (Erb et al. 2006a), we rely on extrapolation of the observed relations and metallicities derived from emission line diagnostics. We assume that metallicities determined from emission and absorption lines are the same, and that there are no metallicity gradients. The luminosity metallicity relation in Tremonti et al. (2004) shifts by 0.35 dex in metallicity relative to the relation for galaxies at $z \sim 2$ (Erb et al. 2006a). This relation suggests that a 10% solar metallicity DLA galaxy has $U \sim 31$ mag, i.e. well below the detection limit of our data, while a 0.4 solar metallicity sub-DLA has $U \sim 28$ mag.

For the strong Mg II absorber towards Q1408, we can only estimate the metallicity from the $W_r^{\mathrm{Mg\,II}\lambda 2796}$ calibration in Turnshek et al. (2005) and Murphy et al. (2007). This calibration gives –0.9 < [M/H] < –0.7, provided that the cloud is a DLA system. While higher resolution spectra are needed to investigate the velocity spread, the SDSS spectra indicate that the Mg II line of Q1408 has a width that is 20–30% lower than in Q1108. Hence the metallicity could be lower, and the absorbing galaxy should be fainter than that towards Q1108.

6. Discussion and summary

Using the absorption of background QSO light by intervening DLAs at $z > 3$, we look for the galaxies responsible for intervening strong Mg II systems at $z \approx 2$ along two lines of sight. The velocity spreads and equivalent widths of the absorption lines indicate that the strong Mg II systems are possible DLAs. Very deep images obtained for these two QSOs reveal no galaxies directly in the line of sight to a limiting magnitude of $U_{\mathrm{AB}} = 28.0$. The most nearby objects are located at impact parameters of ~5″, corresponding to about 40 kpc at $z \approx 2$. While no point sources are found close to the lines of sight, we find evidence for the presence of a more extended structure in a smoothed U band image of the field of Q1408. This structure has a much smaller impact parameter of 0.″8 or 7 kpc at $z \approx 2$. Such extended low surface brightness objects would be impossible to detect after PSF subtraction of the bright background QSOs.

We consider two possible reasons for the non detections of nearby point sources. Either the galaxies are too faint, or the impact parameters are large. The first possibility, that the galaxies are very faint and below the detection limit, is in agreement with low metallicity absorbers. However, this hypothesis must be justified based on several assumptions and extrapolations.

Firstly, since the metallicities cannot be measured exactly because the Lyα absorption lines lie in the absorbed part of the QSO spectra, we have to rely on the correlation between DLA/sub-DLA metal-line velocity width and metallicity to estimate [M/H]. Secondly, we must assume that the objects are DLAs, and not LLS which generally have larger metallicities for a given absorption line width. Finally, we must extrapolate the metallicity luminosity relation observed for DLAs. These assumptions lead to an expected magnitude of the galaxy below the detection limit.

The closest galaxies to the line of sight of the QSOs are located at 40 kpc. They have luminosities of 0.03 L^* and 0.3L^* corresponding to SFR of 0.5 and 4.9 $M_\odot$ yr^{-1}, respectively for the Q1108 and Q1408 fields assuming that the redshifts are indeed $z \approx 2$. The luminosities are in agreement with Rao et al. (2003), who found that Mg II absorbers at $z < 1$ arise in 0.1 L^* galaxies, but in contrast to the results in O'Meara et al. (2006), who found brighter galaxies (0.3–1.2L^* within 25 kpc) for two different fields at $z \approx 2$. In comparison, the strong Mg II galaxies which intervene the sight lines to GRBs are of similar luminosities than in the objects in the two FORS fields, but are typically found at smaller impact parameters (Pollack et al. 2009). The galaxies studied by O'Meara et al. (2006) could, however, be at lower redshift than the absorption systems. Spectroscopic confirmation in these four fields including ours would be of great interest. The SFRs we derive for the two fields are similar to those determined from spectroscopic observations of the galaxies responsible for strong Mg II systems at lower redshifts ($0.8 < z < 1$) (Bouché et al. 2007), but these galaxies are generally found at smaller impact parameters (20 ± 12 kpc).

While the impact parameters for the two closest objects are larger than the size of neutral gas discs in high redshift gas rich (proto)-galaxies as estimated in simulations (Nagamine et al. 2007), observational results in this area is still very limited. The kinematics of high redshift DLAs are inconsistent with a large rotating disc scenario (Zwaan et al. 2008). In order to explain the larger velocities of high redshift DLAs relative to local H I discs, there may be a population of DLAs that arise in starburst winds or from tidal interactions of galaxies, just as hypothesised for strong Mg II systems (Bond et al. 2001; Bouché et al. 2007). Clouds with DLA column densities can be located several tens of kpc from the galaxy centre as seen from observations (Ellison et al. 2007) which is also supported by simulations of the halos of massive galaxies at redshifts $z = 3$ (Pontzen et al. 2008).

In order to investigate whether the Mg II absorption systems are associated with the low luminosity galaxies at a considerable impact parameter, spectroscopic data of the galaxies are necessary, which is challenging due to their faintness. Nevertheless, the Lyα fluxes for pure emission line objects are within the reach of current spectrographs. Specifically, IFU observations are useful in the search for Lyα emission lines very near to the QSO lines of sight, and especially when the objects are extended. Such observations can simultaneously be used to determine the redshifts of the other galaxies within 10″ of the line of sight to the QSOs.

Acknowledgements. We thank Sebastian Lopez for sharing the UVES data, and the referee for a thoughtful and detailed report. P.N. acknowledges support from the French Ministry of European and Foreign Affairs.

References

Adelberger, K. L., Steidel, C. C., Shapley, A. E., et al. 2004, ApJ, 607, 226
Bond, N. A., Churchill, C. W., Charlton, J. C., et al. 2001, ApJ, 562, 641
Bouché, N., Murphy, M. T., Péroux, C., Csabai, I., & Wild, V. 2007, New Astron. Rev., 51, 131
Bruzual, G., & Charlot, S. 2003, MNRAS, 344, 1000
Chen, H.-W., & Tinker, J. L. 2008, ApJ, 687, 745
Chen, H.-W., Perley, D. A., Pollack, L. K., et al. 2009, ApJ, 691, 152
Christensen, L., Wisotzki, L., Roth, M. M., et al. 2007, A&A, 468, 587
Colbert, J. W., & Malkan, M. A. 2002, ApJ, 566, 51
Dall'Aglio, A., Wisotzki, L., & Worseck, G. 2009, [arXiv:0906.1484]
Dessauges-Zavadsky, M., Calura, F., Prochaska, J. X., D'Odorico, S., & Matteucci, F. 2004, A&A, 416, 79
Dessauges-Zavadsky, M., Calura, F., Prochaska, J. X., D'Odorico, S., & Matteucci, F. 2007, A&A, 470, 431
Dessauges-Zavadsky, M., Ellison, S. L., & Murphy, M. T. 2009, MNRAS, 396, L61
Ellison, S. L. 2006, MNRAS, 368, 335
Ellison, S. L., Hennawi, J. F., Martin, C. L., et al. 2007, MNRAS, 378, 801
Ellison, S. L., Murphy, M. T., & Dessauges-Zavadsky, M. 2009, MNRAS, 392, 998
Erb, D. K., Shapley, A. E., Pettini, M., et al. 2006a, ApJ, 644, 813
Erb, D. K., Steidel, C. C., Shapley, A. E., et al. 2006b, ApJ, 646, 107
Fukugita, M., Shimasaku, K., & Ichikawa, T. 1995, PASP, 107, 945
Fynbo, J. U., Møller, P., & Warren, S. J. 1999, MNRAS, 305, 849

Fynbo, J. P. U., Prochaska, J. X., Sommer-Larsen, J., Dessauges-Zavadsky, M., & Møller, P. 2008, ApJ, 683, 321
Gabasch, A., Bender, R., Seitz, S., et al. 2004, A&A, 421, 41
Gabasch, A., Hopp, U., Feulner, G., et al. 2006, A&A, 448, 101
Grazian, A., Fontana, A., de Santis, C., et al. 2006, A&A, 449, 951
Grove, L. F., Fynbo, J. P. U., Ledoux, C., et al. 2009, A&A, 497, 689
Haehnelt, M. G., Steinmetz, M., & Rauch, M. 1998, ApJ, 495, 647
Haehnelt, M. G., Steinmetz, M., & Rauch, M. 2000, ApJ, 534, 594
Heinmüller, J., Petitjean, P., Ledoux, C., Caucci, S., & Srianand, R. 2006, A&A, 449, 33
Jakobsson, P., Hjorth, J., Fynbo, J. P. U., et al. 2004, A&A, 427, 785
Kacprzak, G. G., Churchill, C. W., Steidel, C. C., & Murphy, M. T. 2008, AJ, 135, 922
Kennicutt, R. C. 1998, ARA&A, 36, 189
Kinney, A. L., Calzetti, D., Bohlin, R. C., et al. 1996, ApJ, 467, 38
Kulkarni, V. P., Woodgate, B. E., York, D. G., et al. 2006, ApJ, 636, 30
Ledoux, C., Petitjean, P., Bergeron, J., Wampler, E. J., & Srianand, R. 1998, A&A, 337, 51
Ledoux, C., Petitjean, P., Fynbo, J. P. U., Moller, P., & Srianand, R. 2006, A&A, 457, 71
Meiring, J. D., Lauroesch, J. T., Kulkarni, V. P., et al. 2009, MNRAS, 397, 2037
Møller, P., & Warren, S. J. 1993, A&A, 270, 43
Møller, P., Warren, S. J., Fall, S. M., Fynbo, J. U., & Jakobsen, P. 2002, ApJ, 574, 51
Møller, P., Fynbo, J. U., & Fall, S. M. 2004, A&A, 422, L33
Murphy, M. T., Curran, S. J., Webb, J. K., Ménager, H., & Zych, B. J. 2007, MNRAS, 376, 673
Nagamine, K., Wolfe, A. M., Hernquist, L., et al. 2007, ApJ, 660, 945
Nestor, D. B., Turnshek, D. A., Rao, S. M., et al. 2007, ApJ, 658, 185
Noterdaeme, P., Petitjean, P., Ledoux, C., et al. 2009, A&A, [arXiv:0908.1574]
O'Meara, J. M., Chen, H.-W., & Kaplan, D. L. 2006, ApJ, 642, L9
Osterbrock, D. E. 1989, Astrophysics of gaseous nebulae and active galactic nuclei (Mill Valley, CA: University Science Books)
Péroux, C., Dessauges-Zavadsky, M., D'Odorico, S., Kim, T., & McMahon, R. G. 2003, MNRAS, 345, 480
Patat, F. 2003, A&A, 400, 1183
Péroux, C., Meiring, J. D., Kulkarni, V. P., et al. 2008, MNRAS, 386, 2209
Pettini, M., Smith, L. J., Hunstead, R. W., et al. 1994, ApJ, 426, 79
Pettini, M., Ellison, S. L., Steidel, C. C., et al. 1999, ApJ, 510, 576
Pollack, L. K., Chen, H. W., Prochaska, J. X., et al. 2009, ApJ, 701, 1605
Pontzen, A., Governato, F., Pettini, M., et al. 2008, MNRAS, 390, 1349
Prochaska, J. X., & Wolfe, A. M. 1997, ApJ, 487, 73
Prochaska, J. X., & Wolfe, A. M. 2009, ApJ, 696, 1543
Prochaska, J. X., Henry, R. B. C., O'Meara, J. M., et al. 2002, PASP, 114, 933
Prochaska, J. X., Gawiser, E., Wolfe, A. M., Cooke, J., & Gelino, D. 2003, ApJS, 147, 227
Prochaska, J. X., Herbert-Fort, S., & Wolfe, A. M. 2005, ApJ, 635, 123
Prochaska, J. X., Chen, H.-W., Wolfe, A. M., Dessauges-Zavadsky, M., & Bloom, J. S. 2008, ApJ, 672, 59
Rao, S. M., & Turnshek, D. A. 2000, ApJS, 130, 1
Rao, S. M., Nestor, D. B., Turnshek, D. A., et al. 2003, ApJ, 595, 94
Rao, S. M., Turnshek, D. A., & Nestor, D. B. 2006, ApJ, 636, 610
Rauch, M., Haehnelt, M., Bunker, A., et al. 2008, ApJ, 681, 856
Savage, B. D., & Sembach, K. R. 1991, ApJ, 379, 245
Schlegel, D. J., Finkbeiner, D. P., & Davis, M. 1998, ApJ, 500, 525
Schneider, D. P., Hall, P. B., Richards, G. T., et al. 2007, AJ, 134, 102
Shapley, A. E., Steidel, C. C., Pettini, M., et al. 2003, ApJ, 588, 65
Shapley, A. E., Steidel, C. C., Pettini, M., Adelberger, K. L., & Erb, D. K. 2006, ApJ, 651, 688
Smith, H. E., Cohen, R. D., Burns, J. E., Moore, D. J., & Uchida, B. A. 1989, ApJ, 347, 87
Steidel, C. C. 1995, in QSO Absorption Lines, ed. G. Meylan, 139
Steidel, C. C., & Hamilton, D. 1992, AJ, 104, 941
Steidel, C. C., Pettini, M., & Hamilton, D. 1995, AJ, 110, 2519
Steidel, C. C., Adelberger, K. L., Shapley, A. E., et al. 2003, ApJ, 592, 728
Tescari, E., Viel, M., Tornatore, L., et al. 2009, MNRAS, 764
Tremonti, C. A., Heckman, T. M., Kauffmann, G., et al. 2004, ApJ, 613, 898
Turnshek, D. A., Rao, S. M., Nestor, D. B., Belfort-Mihalyi, M., & Quider, A. M. 2005, in Probing Galaxies through Quasar Absorption Lines, ed. P. Williams, C.-G. Shu, & B. Menard, IAU Colloq., 199, 104
Warren, S. J., Møller, P., Fall, S. M., et al. 2001, MNRAS, 326, 759
Weatherley, S. J., Warren, S. J., Møller, P., et al. 2005, MNRAS, 358, 985
Wolfe, A. M., & Chen, H.-W. 2006, ApJ, 652, 981
Wolfe, A. M., Turnshek, D. A., Smith, H. E., et al. 1986, ApJS, 61, 249
Wolfe, A. M., Lanzetta, K. M., Turnshek, D. A., et al. 1992, ApJ, 385, 151
Wolfe, A. M., Howk, J. C., Gawiser, E., Prochaska, J. X., & Lopez, S. 2004, ApJ, 615, 625
Wolfe, A. M., Gawiser, E., & Prochaska, J. X. 2005, ARA&A, 43, 861
Wolfe, A. M., Prochaska, J. X., Jorgenson, R. A., et al. 2008, ApJ, 681, 881
Zwaan, M., Walter, F., Ryan-Weber, E., et al. 2008, AJ, 136, 2886